On Angular Sampling Intervals for Reconstructing Wideband Channel Spatial Profiles in Directional Scanning Measurements

Fan, Wei; Zhang, Fengchun; Wang, Zhengpeng ; Jensen, Ole Kiel; Pedersen, Gert Frølund

Published in:
I E E E Transactions on Vehicular Technology

DOI (link to publication from Publisher):
10.1109/TVT.2020.3030029

Publication date:
2020

Document Version
Accepted author manuscript, peer reviewed version

On Angular Sampling Intervals for Reconstructing Wideband Channel Spatial Profiles in Directional Scanning Measurements

Wei Fan, Fengchun Zhang, Zhengpeng Wang, Ole K. Jensen and Gert F. Pedersen

***Abstract*—Directional scanning measurement is the dominant strategy taken to measure channel spatial profiles for millimeter wave (mmWave) frequency bands. The focus of the paper is on wideband channel spatial profile reconstruction and angular sampling interval (ASI) selection for directional scanning measurement. We propose to employ the trigonometric interpolation technique to reconstruct the spatial channel profile and to use Nyquist sampling theorem and spherical wave mode theory to determine the ASI. Our analysis demonstrated that the half-power beam width (HPBW) of the antenna is a good approximation for the ASI setting to ensure accurate directional scanning measurements. The reconstructed power-angle-delay profile (PADP), composite power angular spectrum (PAS), delay and angle characteristics match well with those of the target in the measured data when the ASI is set to the antenna HPBW.**

***Index Terms*—Radio channel sounding, directional scanning, trigonometric interpolation, spherical wave modes.**

I. Introduction

Millimeter wave (mmWave) communication has been seen as an enabling technique for the fifth generation (5G) cellular systems, while terahertz (THz) frequency is envisioned as a key wireless technology for 5G beyond [1]. Understanding how radio signal propagates in the deployment scenario is the key to the design and development of wireless systems, which requires reliable radio channel sounding data.

Directional channel scanning, either based on mechanically rotatable directive antennas with the help of a turntable [2], [3] or electrically-steerable antennas [4], [5], has been the dominant solution to measure the channel at high frequency bands. This is mainly due to the high gain (thus a large measurement distance), low cost and simplicity offered by the directional scanning systems. Numerous works have been reported based on the directive scanning measurements. In [6], [7], different techniques to estimate the omni-directional path loss model from the directional scanning measurements were validated. [8] investigated how to reconstruct the power delay profile seen by an omni-directional antenna based on directional scanning measurements. A technique was proposed in [9] to de-embed the antenna pattern from captured channel profiles to obtain propagation channel. In [10], it was numerically demonstrated that the multipath parameter estimation accuracy is related to the ratio of the antenna half power beamwidth (HPBW) to the angular sampling interval (ASI). For directional scanning measurements, measured channel spatial profiles are affected by the measurement antennas in two aspects. The first one is introduced by non-ideal antenna radiation pattern (i.e. wide beamwidth for the main beam and undesired high side-lobes) [9], [10]. In practical measurements, antenna pattern of the measurement antenna often cannot be de-embedded from the measured data easily. Therefore, main beam width and side-lobe levels should be carefully considered when selecting the measurement antenna. The second aspect is related to the ASI selection, which is the main focus of this work.

For directional scanning measurements, the selection of the ASI is a trade off between measurement time and accuracy. It is not wise to waste time and effort for too high oversampling. Hence, it is highly important to provide solid theoretical view to this parameter choice, which is often selected based on experience and some rules of thumb in the literature. The choice of the ASI is typically determined by the directivity of antenna. For example, approximately half of the HPBW in [1]–[3], [6], and approximately the same as HPBW in [7] were reported for the ASI setting, respectively. To ensure that sufficient angular samples are available, a popular strategy is to set a much smaller ASI than the HPBW (e.g. 0.5^{o} or 1^{o} scanning step), see e.g. in [9], [11], [12].

However, no detailed theoretical and experimental analysis has been reported on how to select the ASI for directional scanning measurement. Furthermore, it is also unclear how wideband spatial channel characteristics, e.g. power-angle-delay profile (PADP), wideband power, delay and angle parameters, would be affected by the ASI setting, to the best knowledge of the authors.

In this paper, we attempt to address this aspect by employing the well-known trigonometric interpolation technique, which is used to reconstruct antenna radiation pattern and channel spatial profile. We further propose to determine the ASI based on the Nyquist sampling criteria and spherical wave mode theory. The impact of ASI selection is further validated with simulated and measured horn antenna patterns, and measured spatial channel profiles. To evaluate the performance of the interpolation algorithm and its dependence on ASI selection, the interpolated results (with various ASI settings) are compared to those with a much higher angular resolution (i.e. a small ASI setting) in the simulated and measured results.

The rest of this paper is structured as follows. In Section II, the principle of trigonometric interpolation for channel spatial profile reconstruction is described. Section III describes the

Wei Fan, Fengchun Zhang, Ole K. Jensen and Gert F. Pedersen are with the Antenna Propagation and Millimeter-wave Systems (APMS) section, Department of Electronic Systems, Aalborg University, 9220 Aalborg, Denmark.

Zhengpeng Wang is Electronics and Information Engineering, Beihang University, Beijing, 100191, China

application of Nyquist sampling theorem and spherical wave mode theory for ASI determination, and discusses mode number selection (i.e. ASI selection) rule for directional scanning measurement. In Section IV, the dependence of the interpolation performance on ASI selection is investigated for the measured horn antenna pattern and wideband channel spatial profiles. The impact of ASI selection on channel parameter accuracy is also presented in Section IV. The conclusion is provided in Section V.

II. Trigonometric Interpolation

For antenna pattern interpolation, many methods have been proposed in the literature, e.g. the effective aperture distribution function (EADF) method [13], [14] and trigonometric interpolation method [15]. In this paper, we address this problem with the trigonometric interpolation method, due to the fact that antenna patterns and channel spatial profiles are periodic functions.

For simplicity, the discussion in the paper is focused on one dimension (1D) interpolation (i.e. azimuth domain only), though the extension to 2D interpolation (i.e. both azimuth and elevation domain) is straightforward.

The 1D gain pattern of an antenna $g(\theta)$ can be approximated by a discrete set of data as:

$$g(\theta) = a_0 + \sum_{n=1}^{N} a_n \cos(n\theta) + \sum_{n=1}^{N} b_n \sin(n\theta),\ \theta \in [0, 2\pi] \quad (1)$$

where $\{a_0, a_1, ..., a_N\}$ and $\{b_1, ..., b_N\}$ are the $2N+1$ unknown coefficients. The $2N+1$ coefficients can be solved once $2N+1$ samples, $g(\theta_n)$, are available. More specifically, since the scanned directions (i.e. discrete samples) are typically equally spaced in practice, the solution of the $2N+1$ coefficients can be directly given by its discrete Fourier transform. How well the interpolated antenna pattern approximates its true pattern is determined by the number of samples $2N+1$ with ASI $= 360^o/(2N+1)$. We propose to determine the ASI based on the Nyquist sampling and spherical wave mode theory.

III. ASI Determination

Horn antennas are dominantly employed in the directional scanning measurement. Therefore, we use the horn antenna as an example in our numerical analysis. The horn antenna can be approximated by the TE_{10} mode rectangular aperture, i.e. assuming constant phase over the aperture and infinite ground plane [16]. The far field E-fields and the HPBW can be directly calculated according to the Table 12.1 in [16] for the TE_{10} mode aperture distribution on the ground plane. To mimic the horn antennas employed in the measurement (as explained later), the dimensions of the rectangular aperture $a = 3.2\lambda$ and $b = 3\lambda$ are set. Following formulas in Table 12.1 in [16], the HPBW of the antenna is 21^o for the H-plane and 17^o for the E-plane, respectively. The vertically polarized antenna gain pattern and its azimuth cut (i.e. with $\phi = 0^o$) are shown in Fig. 1 and Fig. 2, respectively. The HPBW of the pattern in Fig. 2 is 21^o, which agrees well with the theory.

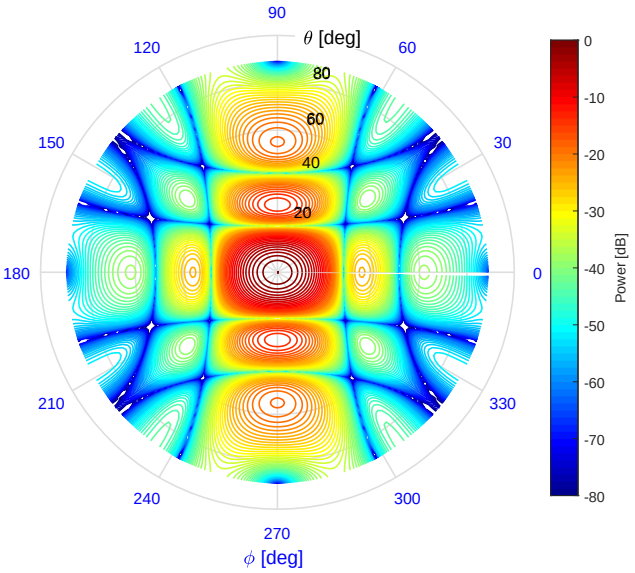

Figure 1. Polar contour plot of the normalized antenna pattern [17]. The actual antenna gain is 18.7 dBi. $\phi = 0^o/180^o$ denotes the azimuth cut (H-plane).

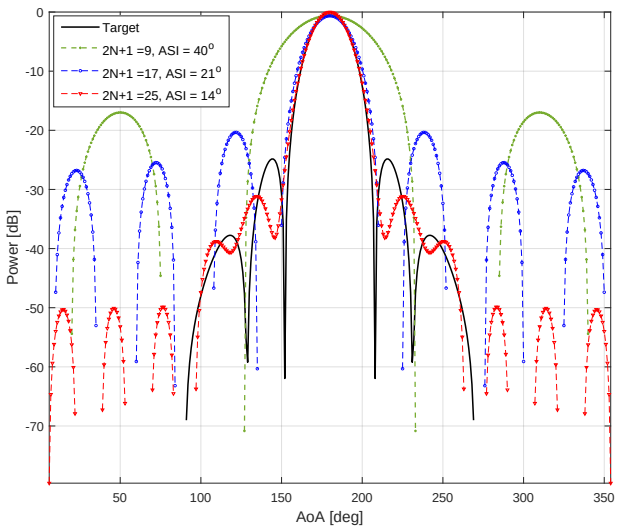

Figure 2. The azimuth cut of the normalized antenna pattern and the interpolated antenna patterns with different ASIs.

A. Nyquist sampling theorem

According to the Nyquist sampling theorem, the antenna pattern can be exactly reproduced, if we sample at least twice of the maximum mode (i.e. harmonics) in the trigonometric mode spectrum of the antenna pattern. The mode spectrum can be obtained via performing Fourier transform of the antenna pattern, as shown in Fig. 3. As explained, the $2N+1$ mode coefficients $\{a_0, a_1, ..., a_N\}$ and $\{b_1, ..., b_N\}$ can be directly given by the discrete Fourier transform. Note that only mode coefficients $|a_n|$ are plotted, since we have $|b_n| = 0$ due to the symmetry of the antenna pattern. To perfectly reconstruct the antenna pattern, N approaching infinite would be required. However, as shown in Fig. 3, the mode coefficients drop off rapidly. The accumulated power of $N = 4$, 8 and 12 modes

is 67%, 96% and 99.8%, respectively. We can select $N = 4$, 8, and 12, and reconstruct the antenna pattern following the trigonometric interpolation (1), as shown in Fig. 2. With $N = 8$, the reconstructed antenna pattern matches well with the target one with a 20 dB range, with 0.6 dB drop in main beam direction and slightly wider bandwidth. A large deviation exists with $N = 4$, compared to a good match achieved with $N = 12$ with the 30 dB range. This analysis indicates that $N = 8$, i.e. ASI set to the HPBW 21°, is a good approximation for directional scanning measurements, though a better accuracy would require a smaller ASI setting.

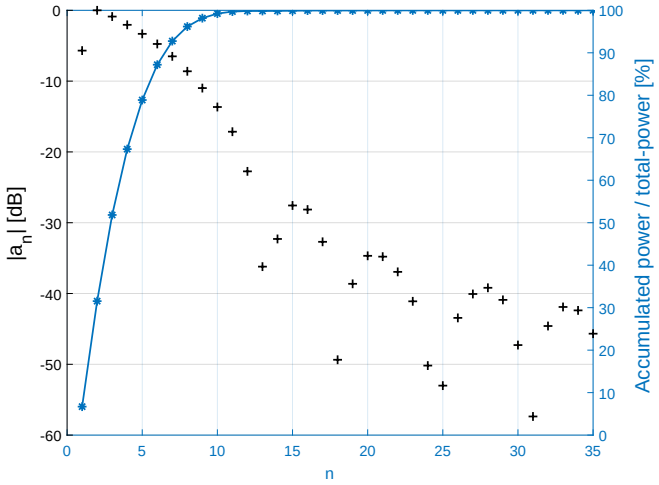

Figure 3. Trigonometric mode spectrum of the antenna pattern and accumulated power percentile.

The discussion can be applied for asymmetrical directive antenna patterns in principle. For asymmetrical case, the magnitudes of both b_n and a_n would decrease as the mode index in the mode spectrum goes up, resulting in limited number of dominant modes. Directive antennas employed in practical measurements are typically symmetric horn-type antennas, which highly resemble the simulated antenna with its radiation pattern shown in Fig. 1. Note that the accumulated power is used as the metric to determine the ASI in the paper, which has not been reported in the literature. For practical measurements, it would be good to know a rule of thumb to determine the ASI. We have shown that around 95% of total accumulated power (i.e. the majority of the power) is accounted for, if the HPBW is selected as the ASI. Same analysis is also performed for synthetic directive antennas according to the 3GPP specification [18], and similar conclusions have been reached.

B. Spherical wave mode analysis

Alternatively, the number of modes or ASI can be determined based on the spherical wave mode analysis as well. According to [19], the radiation pattern of any antenna with a fixed size can be described with a finite series of spherical wave modes, which can be given by an empirical rule as:

$$K = [\frac{2\pi}{\lambda} r_o] + k_1, \tag{2}$$

where $[\cdot]$ is the ceiling function, r_o is the radius of the minimum sphere that circumscribes the antenna, and λ is the wavelength. k_1 is the accuracy parameter, which is a small integer typically ranging from 0 to 10 [19]. This is the well-known cut-off property of spherical modes (i.e. only modes with $K < \frac{2\pi}{\lambda} r_o$ are of importance since higher modes are heavily attenuated). According to (2), the number of required modes is $K = [\frac{2\pi}{\lambda} r_o] + k_1 = [2\pi \frac{\sqrt{(3^2+3.2^2)}}{2}] + k_1 = 14 + k_1$ Therefore, the number of required samples $(2K+1)$ calculated following (2) is significantly larger than that obtained when the ASI is set to the HPBW. Note that (2) is employed to ensure accurate antenna pattern measurements, where accurate measurement of all antenna parameters, e.g. the antenna main beam, side-lobe levels, nulls and cross polarization ratio of the antenna, are targeted. However, the main objective of our work is only to detect direction and power of impinging signals in directional scanning measurements, whose accuracy is mainly ruled by the antenna main beam if the side-lobes are insignificant. As explained in the introduction, the measured PAS would be affected by high sidelobes of the directive antenna, which cannot easily be de-embedded from the measured data. It is often required that the employed antenna should have a low sidelobe level (SLL), e.g. less than -20 dB as shown in Fig. 2, to reduce the influence of the sidelobes. Therefore, the measurement accuracy is mainly ruled by the antenna main beam and the required number of modes will be consequently smaller than that determined by (2).

A more reasonable criteria is to evaluate whether all dominant spherical wave modes are accounted for when selecting the number of modes. Once the E-fields are calculated for the rectangular aperture, we can obtain the mode power spectrum using the standard spherical near-field to far-field transformation tool [19], as shown in Fig. 4. We can clearly observe that all modes larger than $K = 14$ are significantly attenuated (black plus signs), which justifies the cut-off property as expected. The first eight modes combined account for 94% of total power, which indicates that the majority of the power is covered if the HPBW is selected as the ASI. Therefore, although $K = 8$ violates the rule of thumb for accurate antenna pattern measurement, it could be a good approximation for directional scanning measurement. As a summary, we can reach a consistent selection on ASI using both the Nyquist sampling and spherical wave mode theory.

C. Mode number selection discussion

As discussed, the cut-off property in (2) is employed to determine the number of samples in order to accurately obtain all antenna pattern parameters (including main beam, sidelobes, backlobes, nulls, etc). Fewer samples (determined by the total accumulated power) are sufficient due to the fact that mainly the main beam pattern should be accurately measured for directional scanning measurements.

For the trigonometric mode spectrum of the antenna pattern (i.e. the Fourier transform of the antenna pattern), the spectrum of the azimuth-pattern (H-plane pattern) is determined from the azimuth cut alone. For 2D case, we would need a 2D trigonometric interpolation of the 2D antenna pattern. The

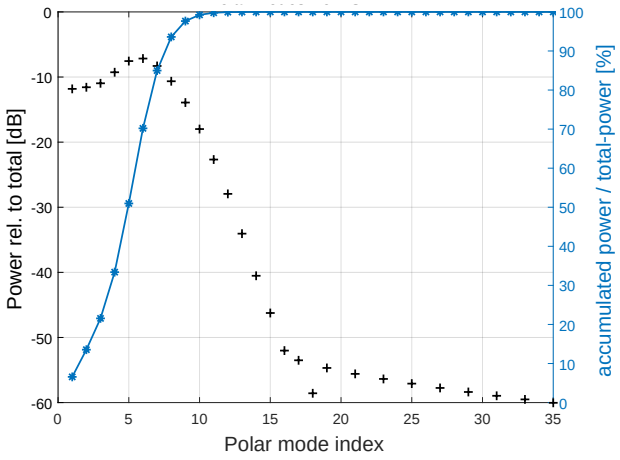

Figure 4. Mode power spectrum and accumulated power percentile for the rectangular aperture.

dominant modes can be then found following the Nyquist sampling theorem from the 2D trigonometric mode spectrum. For antenna measurement, according to spherical near field antenna measurement theory [19], the total number of required modes is given by $K_0 = 2K(K+1)$ with K calculated by (2). To determine the required spherical wave modes for 2D spatial channel reconstruction, we need to consider both the polar mode and azimuthal mode spectrum of the field to ensure that the majority of the accumulated power is accounted for by selecting the dominant modes.

IV. Experimental Validations

A directional scanning measurement in an indoor basement was reported in [12] and summarized below. The measurement system consists of a vector network analyzer (VNA), a local oscillator (LO)/intermediate frequency (IF) distribution unit, and two reference mixer modules, as illustrated in Fig. 5. The mixer module is used to down-convert the received mmWave signals at the Rx to a lower frequency to reduce the cable transmission loss (thus to improve the dynamic range). Both measurements in the line-of-sight (LOS) and obstructed LOS (OLOS) scenarios were carried out. In the OLOS scenario, a metallic plate was placed between the transmit (Tx) antenna and receive (Rx) antenna to block the paths in LOS directions. A VNA equipped with an omni-directional vertically polarized Biconical antenna (Tx) and a directive vertically polarized horn antenna (Rx) were employed to record the channel frequency response. The gain of the Tx antenna and the Rx antenna at 29 GHz is 6 dBi and 19 dBi, respectively. The Rx antenna was rotated in the center of an automated turntable with 720 steps, i.e. with a rotation step of 0.5^o. The frequency range is 28 GHz to 30 GHz using a total of 750 points for each scanning direction, i.e. a frequency resolution of 2.67 MHz. The delay resolution is 0.5 ns, which corresponds to a 0.15 m distance resolution. The horn antenna has 21^o HPBW in the H-plane. The measured horn antenna pattern was extracted from the PAS corresponding to the LOS path, as shown in Fig. 6. Note that the measured antenna pattern slightly differs from the one in data sheet due to distortion introduced by the cable effect in the setup.

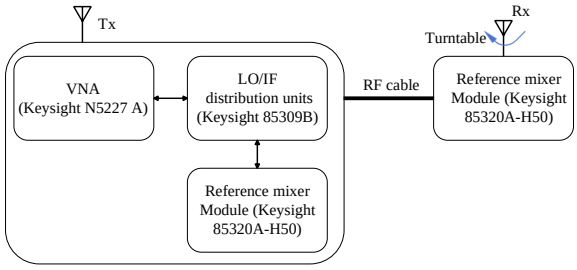

Figure 5. An illustration of the measurement system.

A. Antenna pattern

The interpolated antenna patterns together with the true antenna pattern for the Rx antenna are shown in Fig. 6. Note that the antenna patterns are normalized by the maximum gain of the Rx antenna. As we can see, with a large ASI setting (i.e. ASI $> 21^o$), the main beams of the reconstructed patterns are wider than that of the target, leading to errors in the channel parameters of reconstructed channel (as discussed later). With a small ASI setting (i.e. ASI $\leq 21^o$), we can obtain the same main beam. The smaller ASI we set, the better antenna pattern reconstruction accuracy we can achieve, as expected. With ASI setting at 21^o and 10^o, the reconstructed antenna pattern matches well with the target one with 20 dB range and more than 30 dB range, respectively, which is consistent with our analysis in Section III-A.

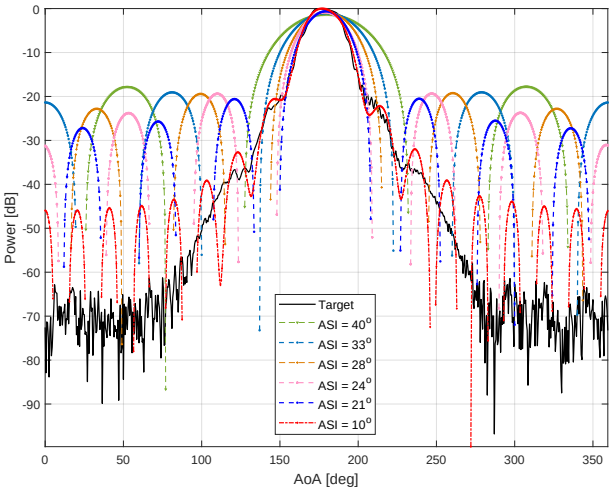

Figure 6. The measured and reconstructed horn antenna patterns with various ASIs.

B. PADP

For spatial channel sounding with a large system bandwidth, we can assume that multipath components are distinguishable in the delay domain. At each delay index, the multipath component is spatially sampled by the rotational directional antenna. The spatial power pattern at each delay index is

therefore only a scaled (multipath gain) and rotated (multipath impinging angle) version of the antenna pattern. Therefore, we can apply the trigonometric interpolation technique for wideband spatial channel reconstruction. In the measurement, the recorded PADP samples of the channel can be denoted by $\mathbf{P}(\tau, \phi) \in \mathbb{R}^{N_\tau \times N_\phi}$ with N_τ and N_ϕ denoting the number of delay indexes and azimuth angle indexes, respectively. The interpolation of the measured PADP $\mathbf{P}(\tau, \phi)$ can be implemented via applying the discussed trigonometric interpolation to PAS at each delay index. The measured PADPs discussed below are normlized by the maximum gain of both the Tx antenna and the Rx antenna, i.e. 25 dBi de-embedded from the measured patterns. As explained in the introduction, the measured channel spatial profiles are affected by the measurement antenna radiation pattern. Some works have been reported in the literature to de-embed the antenna pattern from the measured data [9], while in most cases it is inherently included in the measurement. This is based on the assumption that the measurement antenna has insignificant side-lobes and narrow main beam patterns [7], [12]. The focus of this work is on how to select ASIs, which is another important aspect for directive scanning measurement, while the impact of measurement antenna on the measured channel PAS is not covered.

The measured PADP (with ASI = 0.5^o) and interpolated profiles with ASI = 21^o and ASI = 40^o are shown in Fig. 7 for the LOS scenario and in Fig. 8 for the OLOS scenario, respectively. Note that the PADPs with ASI = 21^o and ASI = 40^o are subsets of the measured PADP (with ASI = 0.5^o). In the LOS scenario, both the dominant paths and weak paths can be accurately reconstructed (both power and angle) with ASI = 21^o. This is expected due to the fact that most paths are within 20 dB dynamic range in the LOS scenario compared to the LOS path. In the OLOS scenario, the dominant paths can still be accurately reconstructed, while small deviations exist for weak paths. This is expected, since some weak paths are more than 20 dB less in power compared to the LOS path. As seen in Fig. 6, deviations exist between the reconstructed antenna pattern and the target one with the 35 dB dynamic range with ASI = 21^o. Reconstruction of both the main beam and side lobes of the paths becomes inaccurate with ASI = 40^o for the LOS and OLOS scenario, as shown in Fig. 7 (below) and Fig. 8 (below), respectively.

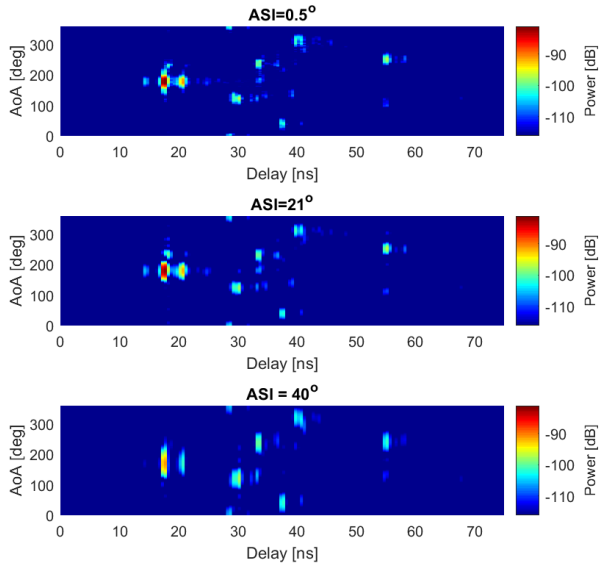

Figure 7. Measured PADP (top) and reconstructed PADP with ASI = 21^o (middle) and ASI = 40^o (below) in the LOS scenario.

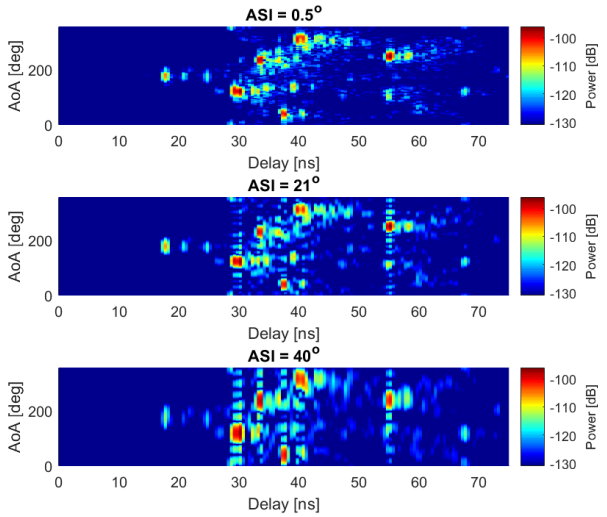

Figure 8. Measured PADP (top) and reconstructed PADP with ASI = 21^o (middle) and ASI = 40^o (below) in the OLOS scenario.

C. Composite PAS

For spatial channel sounding with a narrow-band system, multipath components might not be seperated in the delay domain. The channel impulse response (CIR) measured with a narrow band system is equivelent to the composite CIR obtained via coherent summation of the wideband CIR over the delay domain, i.e., $\mathbf{h}(\phi) = \sum_\tau \mathbf{H}(\tau, \phi)$ with $\mathbf{h}(\phi)$ and $\mathbf{H}(\tau, \phi)$ representing the composite CIR and wide-band CIR, respectively. The composite PAS is thereby obtained by $\mathbf{p}(\phi) = |\mathbf{h}(\phi)|^2$. The composite PAS can be viewed as summation of the complex weighted (i.e. path complex gain) and circularly shifted (i.e. path angle) directive antenna patterns, and therefore its accuracy is ruled by antenna pattern reconstruction accuracy. The target and reconstructed composite PAS for the LOS scenario are shown in Fig. 9 as an example. A good agreement can be achieved within 20 dB if the ASI is set smaller than the antenna HPBW (21^o), while a large deviation exists if ASI is set to 40^o.

D. Channel parameters

Once the wideband spatial profile is reconstructed, all the channel parameters can be calculated and compared with the target channel parameters. The calculation of the total received power, delay characteristics (mean delay and delay spread) and angle characteristics (mean angle and angle spread) is referred to [20], [21] and not detailed here. The deviations of channel parameters between the target (i.e. with ASI = 0.5^o) and reconstructed spatial channel profiles with various ASI settings are summarized in Table I. Compared to the

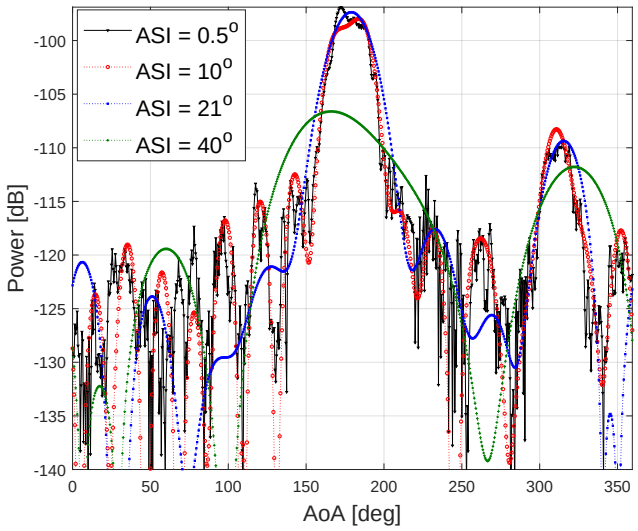

Figure 9. The target and reconstructed composite PAS for the LOS scenario with different ASIs.

OLOS scenario, the LOS scenario presents higher wideband power, smaller mean delay, delay spread and angle spread, as expected. Good accuracy can be achieved if the ASI is set to be smaller than 21^{o}, while large deviations are present with ASI = 40^{o}. This observation is also consistent with previous findings.

Table I
CHANNEL PARAMETER DEVIATIONS.

ASI [°] OLOS/LOS	Wideband Power [dB]	Mean delay [ns]	delay spread [ns]	Mean angle [°]	Angle spread [°]
10.5	0.1/0	0/0.2	-0.1/0.3	1.5/1	0/1
21	0.3/0.1	0.2/0.2	0.1/0.3	-9/1.5	0.3/1.4
40	1.7/-5	-2.5/6.1	-1.8/4.2	-37.5/-7.1	1.3/21.7

V. CONCLUSION

The paper proposes to use the trigonometric interpolation scheme to reconstruct wideband channel spatial profiles. To determine the ASI, we resort to the Nyquist sampling theorem and spherical wave mode theory. We demonstrate that if the HPBW is selected as the ASI, around 95% of total power (i.e. the majority of the power) is accounted for. Furthermore, the main beam in the antenna pattern, which is the main factor in directional scanning measurement, is well approximated. Therefore, the setting of ASI to the antenna HPBW is a reasonable approximation in typically directional scanning measurement, although a smaller ASI would be required if a good approximation of an antenna pattern within a larger range ($\geq$ 20 dB) is needed. The reconstructed PADP, delay and angle characteristics match well with those of the target in the measured data when the ASI is set to the antenna HPBW, although the results are slightly deteriorated due to cable effects.

REFERENCES

[1] B. Peng, K. Guan, S. Rey, and T. KÃijrner, "Power-angular spectra correlation based two step angle of arrival estimation for future indoor terahertz communications," *IEEE Transactions on Antennas and Propagation*, vol. 67, no. 11, pp. 7097–7105, Nov 2019.

[2] S. Hur, H. Yu, J. Park, W. Roh, C. U. Bas, R. Wang, and A. F. Molisch, "Feasibility of mobility for millimeter-wave systems based on channel measurements," *IEEE Communications Magazine*, vol. 56, no. 7, pp. 56–63, July 2018.

[3] X. Zhao, S. Li, Q. Wang, M. Wang, S. Sun, and W. Hong, "Channel measurements, modeling, simulation and validation at 32 ghz in outdoor microcells for 5g radio systems," *IEEE Access*, vol. 5, pp. 1062–1072, 2017.

[4] D. Caudill, P. B. Papazian, C. Gentile, J. Chuang, and N. Golmie, "Omnidirectional channel sounder with phased-arrayantennas for 5g mobile communications," *IEEE Transactions on Microwave Theory and Techniques*, vol. 67, no. 7, pp. 2936–2945, July 2019.

[5] C. U. Bas, R. Wang, S. Sangodoyin, D. Psychoudakis, T. Henige, R. Monroe, J. Park, C. J. Zhang, and A. F. Molisch, "Real-time millimeter-wave mimo channel sounder for dynamic directional measurements," *IEEE Transactions on Vehicular Technology*, vol. 68, no. 9, pp. 8775–8789, Sep. 2019.

[6] K. Haneda, S. L. H. Nguyen, J. JÃd'rvelÃd'inen, and J. Putkonen, "Estimating the omni-directional pathloss from directional channel sounding," in *2016 10th European Conference on Antennas and Propagation (EuCAP)*, April 2016, pp. 1–5.

[7] S. Sun, G. R. MacCartney, M. K. Samimi, and T. S. Rappaport, "Synthesizing omnidirectional antenna patterns, received power and path loss from directional antennas for 5g millimeter-wave communications," in *2015 IEEE Global Communications Conference (GLOBECOM)*, Dec 2015, pp. 1–7.

[8] J. Hejselbæk, A. Karstensen, J. Ø. Nielsen, W. Fan, G. Fr *et al.*, "Validation of emulated omnidirectional antenna output using directive antenna data," in *2017 11th European Conference on Antennas and Propagation (EUCAP)*. IEEE, 2017, pp. 131–135.

[9] R. Zhang, Y. Zhou, X. Lu, C. Cao, and Q. Guo, "Antenna deembedding for mmwave propagation modeling and field measurement validation at 73 ghz," *IEEE Transactions on Microwave Theory and Techniques*, vol. 65, no. 10, pp. 3648–3659, Oct 2017.

[10] M. Kim, "Analysis of multipath component parameter estimation accuracy in directional scanning measurement," *IEEE Antennas and Wireless Propagation Letters*, vol. 17, no. 1, pp. 12–16, Jan 2018.

[11] C. Larsson, B. Olsson, and J. Medbo, "Angular resolved pathloss measurements in urban macrocell scenarios at 28 ghz," in *2016 IEEE 84th Vehicular Technology Conference (VTC-Fall)*, Sep. 2016, pp. 1–5.

[12] W. Fan, I. Carton, J. Ø. Nielsen, K. Olesen, and G. F. Pedersen, "Measured wideband characteristics of indoor channels at centimetric and millimetric bands," *EURASIP Journal on Wireless Communications and Networking*, vol. 2016, no. 1, p. 58, 2016.

[13] M. Landmann and G. Del Galdo, "Efficient antenna description for mimo channel modelling and estimation," in *7th European Conference on Wireless Technology, 2004.* IEEE, 2004, pp. 217–220.

[14] S. Haefner, R. Mueller, and R. S. Thomae, "Full 3d antenna pattern interpolation using fourier transform based wavefield modelling," in *WSA 2016; 20th International ITG Workshop on Smart Antennas*. VDE, 2016, pp. 1–8.

[15] A. Zygmund, *Trigonometric series*. Cambridge university press, 2002, vol. 1.

[16] C. A. Balanis, *Antenna theory: analysis and design*. John wiley & sons, 2016.

[17] A. Ludwig, "The definition of cross polarization," *IEEE Transactions on Antennas and Propagation*, vol. 21, no. 1, pp. 116–119, 1973.

[18] G. R. A. N. W. Group *et al.*, "Study on channel model for frequencies from 0.5 to 100 ghz (release 15)," 3GPP TR 38.901, Tech. Rep., 2018.

[19] J. Hald and F. Jensen, *Spherical near-field antenna measurements*. Iet, 1988, vol. 26.

[20] A. Karstensen, W. Fan, F. Zhang, J. Ø. Nielsen, and G. F. Pedersen, "Analysis of simulated and measured indoor channels for mm-wave beamforming applications," *International Journal of Antennas and Propagation*, vol. 2018, 2018.

[21] A. F. Molisch, *Wireless communications*. John Wiley & Sons, 2012, vol. 34.